



CHORUS

This is the accepted manuscript made available via CHORUS. The article has been published as:

Photon coincidence counting in parametric down-conversion: Interference of field-matter quantum pathways

Konstantin E. Dorfman and Shaul Mukamel

Phys. Rev. A **86**, 023805 — Published 3 August 2012

DOI: [10.1103/PhysRevA.86.023805](https://doi.org/10.1103/PhysRevA.86.023805)

Photon Coincidence Counting in Parametric Down Conversion; Interference of Field-Matter Quantum Pathways

Konstantin E. Dorfman* and Shaul Mukamel
University of California, Irvine, California 92697-2025
 (Dated: July 18, 2012)

The coincidence rate in two detectors that register signal and idler photons in parametric down conversion (PDC) is calculated using a quantum description of the radiation field that extends the semiclassical theory to the resonance regime. The signal is given by a *sum over paths*, each involving a pair of sites (molecules) and six radiation field modes. It may not be factorized into amplitudes representing one-site, three-mode paths. All effects of multiple vacuum modes are accounted for by these paths without adding a Langevin noise source. The molecular information is given by a time ordered superoperator Green's function rather than the susceptibility $\chi^{(2)}$ used in the semiclassical theory.

I. INTRODUCTION

The generation and manipulation of entangled light is of fundamental interest in quantum science, quantum computation and engineering. Nearly a century after the celebrated EPR paper [1], there remain a number of open questions regarding the creation of entangled light. Parametric down conversion (PDC) [2, 3] is an important source of entangled photons that found numerous practical applications such as quantum information technology [4, 5], metrology [6], holography [7], communication [8] and lithography [9–11].

The standard calculation of PDC assumes that all relevant field frequencies are off resonant with matter. It is then possible to adiabatically eliminate all matter degrees of freedom and describe the process by an effective Hamiltonian for the field that contains a nonlinear cubic coupling of three modes. All matter information is embedded into a coefficient that is proportional to $\chi^{(2)}$ [12] that is defined by the semiclassical theory of radiation-matter coupling. Langevin quantum noise is added to represent vacuum fluctuations caused by other field modes [13–15] and account for photon statistics.

We present a microscopic theory of type I PDC that addresses entanglement generation in a transparent way. First, it holds both on and off resonance. The resonant case is especially important for potential spectroscopic applications [16], where unique information about entangled matter [17] can be revealed. Other examples are excitons in molecular aggregates and photosynthetic complexes or biological imaging [18]. Second, it properly takes into account the quantum nature of the generated modes through a generalized susceptibility that has a very different behavior near resonance than the semiclassical $\chi^{(2)}$. $\chi^{(2)}$ is derived for two classical fields and a single quantum field. While this is true for the reverse process (sum frequency generation) it does not apply for PDC, which couples a single classical and two quantum modes. Third, macroscopic propagation effects are not

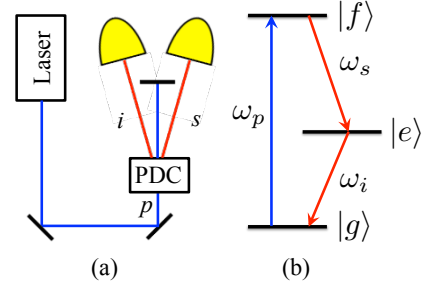


FIG. 1. (Color online) Schematic of the PDC experiment - (a), the three level model system used in our simulations - (b).

required for the basic generation of the signal. Fourth, we include gated detection [19] that yields the finite temporal and spectral resolution of the coincident photons limited by a Wigner spectrogram. For either time or frequency resolved measurement of the generated field, the signal can be expressed as a modulus square of the transition amplitude that depends on three field modes. This is not the case for photon counting.

The nature of entangled light can be revealed by photon correlation measurements that are governed by energy, momentum and/or angular momentum conservation. In PDC, a nonlinear medium is pumped by electromagnetic field of frequency ω_p and some of the pump photons are converted into pairs of (signal and idler) photons with frequencies ω_s and ω_i , respectively (see Fig. 1a) satisfying $\omega_p = \omega_s + \omega_i$.

In the semiclassical approach the process is described by an effective interaction Hamiltonian for the field modes

$$H_{int}(t) = i\hbar \sum_j \int \frac{d\omega_s}{2\pi} \frac{d\omega_i}{2\pi} \frac{d\omega_p}{2\pi} \chi_{+--}^{(2)}(\omega_s, \omega_i, \omega_p) \times \hat{a}^{(s)\dagger} \hat{a}^{(i)\dagger} \beta^{(p)} e^{i\Delta\mathbf{k}(\mathbf{r}-\mathbf{r}_j)} e^{-i(\omega_p - \omega_s - \omega_i)t} + H.c., \quad (1)$$

where $\hat{a}^{\dagger(s)}$ and $\hat{a}^{(i)\dagger}$ are creation operators for signal and idler modes, $\beta^{(p)}$ is the expectation value of the classical pump field, $\Delta\mathbf{k} = \mathbf{k}_p - \mathbf{k}_s - \mathbf{k}_i$, j runs over

* Email: kdorfman@uci.edu

molecules, $\chi_{+--}^{(2)}$, (normally denoted $\chi^{(2)}(-\omega_s; -\omega_i, \omega_p)$) is the second-order nonlinear susceptibility

$$\chi_{+--}^{(2)}(\omega_s = \omega_p - \omega_i, \omega_i, \omega_p) = \left(\frac{i}{\hbar}\right)^2 \int_0^\infty \int_0^\infty dt_2 dt_1 \times e^{i\omega_i(t_2+t_1)+i\omega_p t_1} \langle [[V(t_2+t_1), V(t_1)], V(0)] \rangle + (i \leftrightarrow p). \quad (2)$$

We have introduced superoperator notation that provides a convenient bookkeeping of time ordered Green's functions. With every ordinary operator A we associate two superoperators defined by their action on an ordinary operator X as $A_L = AX$ acting from left, $A_R = XA$ (right). We further define the symmetric and antisymmetric combinations $A_+ = \frac{1}{\sqrt{2}}(A_L + A_R)$, $A_- = \frac{1}{\sqrt{2}}(A_L - A_R)$. Thus, the “+ --” indices in Eq. (2) signify two commutators followed by an anti commutator. The bottom line of the semiclassical approach is that PDC is represented by 3-point matter-field interaction via the second order susceptibility $\chi_{+--}^{(2)}$ that couples the signal, idler and pump modes. However, it has been realized, that other field modes are needed to yield the correct photon statistics. Electromagnetic field fluctuations are then added as quantum noise (Langevin forces) [13].

II. MICROSCOPIC SUPEROPERATOR APPROACH TO PDC

Here we present a fully microscopic calculation of the coincidence count rate in type I PDC [20]. We show that PDC is governed by a quantity that resembles but is different from (2). In contrast with the semiclassical approach, PDC emerges as a 6-mode two-molecule rather than 3-mode matter-field interaction process and is represented by convolution of two quantum susceptibilities $\chi_{LL-}^{(2)}(\omega_s, \omega_i, \omega_p)$ and $\chi_{LL-}^{(2)*}(\omega'_s, \omega'_i, \omega'_p)$ that represent a pair of molecules in the sample interacting with many vacuum modes of the signal (s, s') and the idler (i, i'). Field fluctuations are included self consistently at the microscopic level. Furthermore the relevant nonlinear susceptibility is different from the semiclassical one $\chi_{+--}^{(2)}$ and is given by

$$\chi_{LL-}^{(2)}(\omega_s = \omega_p - \omega_i, \omega_i, \omega_p) = \left(\frac{i}{\hbar}\right) \int_0^\infty \int_0^\infty dt_2 dt_1 \times e^{i\omega_i(t_2+t_1)+i\omega_p t_1} \langle [V(t_2+t_1)V(t_1), V(0)] \rangle + (i \leftrightarrow s). \quad (3)$$

Eq. (3) has a single commutator and is symmetric to a permutation of ω_i and $\omega_s = \omega_p - \omega_i$, as it should. Eq. (2) has two commutators and lacks this symmetry.

Our calculation of the coincidence rate of signal and

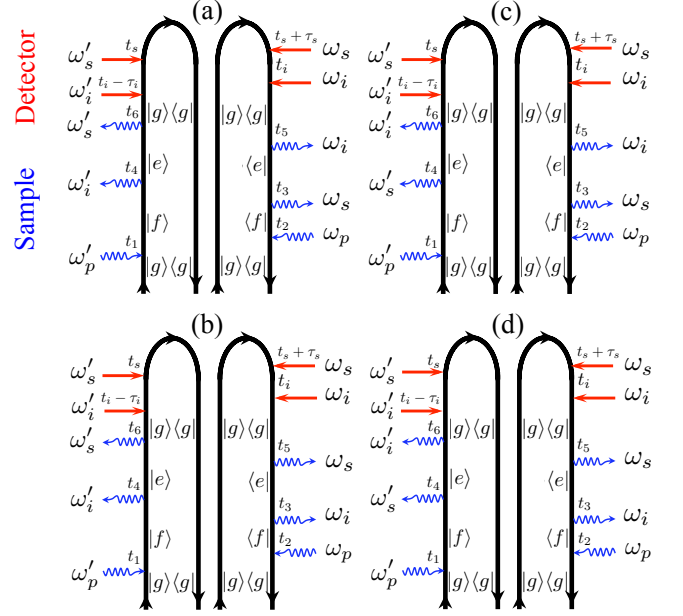


FIG. 2. (Color online) Loop diagrams for the coincidence count rate of signal and idler photons generated in type I PDC (Eq. (5)). The left and right diagrams represent a pair of molecules. Curvy blue (straight red) arrows represent field-matter interaction with the sample (detectors). There are four possible permutations (s/i and s'/i'). This leads to four terms when Eq. (8) is substituted into Eq. (7).

idler photons starts with the definition [14]

$$R_c(\bar{\omega}_s, \bar{t}_s; \bar{\omega}_i, \bar{t}_i) = \int_{-\infty}^\infty dt_s \int_{-\infty}^\infty dt_i \langle E_{tf}^{\dagger(i)}(t_i) E_{tf}^{\dagger(s)}(t_s) E_{tf}^{(s)}(t_s) E_{tf}^{(i)}(t_i) \rangle, \quad (4)$$

where the angular brackets in the correlation function denote $\langle \dots \rangle \equiv \text{tr}(\dots \rho)$ where ρ is the field plus matter density operator. Here E_{tf} is time-and-frequency gated electric field measured by detector, that will be clarified in Section IIB. The gate is characterized by mean frequency $\bar{\omega}_\nu$ and time \bar{t}_ν , ($\nu = s, i$).

A. Bare coincidence rate

We first calculate the “bare” correlation function [19] (no gating) $\langle E^{\dagger(i)}(t'_i) E^{\dagger(s)}(t'_s + \tau_s) E^{(s')}(t'_s) E^{(i')}(t'_i - \tau_i) \rangle$ which represents four spectral modes arriving at the detectors, where modes s, s', i, i' are defined by their frequencies $\omega_s, \omega'_s, \omega_i, \omega'_i = \omega_p - \omega_s, \omega'_s = \omega'_p - \omega'_i$. This is given by a time ordered product of Green's functions of superoperators in the interaction picture

$$\langle \mathcal{T} E_R^{\dagger(i)}(t'_i) E_R^{\dagger(s)}(t'_s + \tau_s) E_L^{(s')}(t'_s) E_L^{(i')}(t'_i - \tau_i) \times e^{-\frac{i}{\hbar} \int_{-\infty}^\infty \sqrt{2} H'_L(\tau) d\tau} \rho(-\infty) \rangle. \quad (5)$$

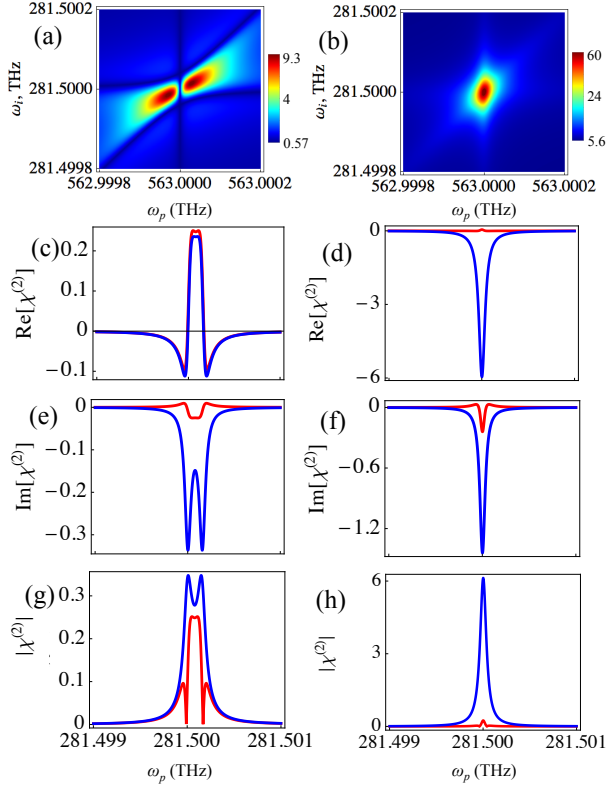


FIG. 3. (Color online) Absolute value of semiclassical susceptibility $|\chi_{+-}^{(2)}(-(\omega_p - \omega_i), -\omega_i, \omega_p)|$ (arb. units) (9) - (a), and quantum the susceptibility $|\chi_{LL-}^{(2)}(-(\omega_p - \omega_i), -\omega_i, \omega_p)|$ (8) - (b) vs pump ω_p and idler frequency ω_i . We used the standard KTP parameters outlined in the text. Left column: real - (c), imaginary part - (e) and absolute value - (g) of $\chi_{+-}^{(2)}$ - red line and $\chi_{LL-}^{(2)}$ - blue line for off resonant pump $\omega_p - \omega_{gf} = 10\gamma_{gf}$. Right column: (d),(f),(h) - same as (c),(e),(g) but for resonant pump $\omega_p \simeq \omega_{gf}$.

The radiation-matter coupling superoperator is

$$H'_-(t) = \sum_{x=s,i,p} \left[E_L^{\dagger(\nu)}(t) V_L(t) - E_R^{\dagger(\nu)}(t) V_R(t) \right] + H.c. \quad (6)$$

$V^\dagger(V)$ is matter raising (lowering) operator so that $V_L(t) = \mu_{gf}|g\rangle\langle f|e^{-i(\omega_{gf} + \gamma_{gf})t} + \mu_{eg}|g\rangle\langle e|e^{-i(\omega_{eg} + \gamma_{eg})t} + \mu_{fe}|e\rangle\langle f|e^{-i(\omega_{fe} + \gamma_{fe})t}$, where μ_{ij} , γ_{ij} , γ_{ij} , and ω_{ij} are corresponding dipole moment, line width and transition frequency of the transition $i \leftrightarrow j$, ($i, j = g, e, f$).

In type I PDC the sample is composed of N identical molecules initially in their ground state. They interact with one classical pump mode and emit two spontaneously generated quantum modes with the same polarization into two collinear cones. The initial state of the optical field is given by $|0\rangle_s|0\rangle_i|\beta\rangle_p$. A classical pump field promotes the molecule from its ground state $|g\rangle$ to the doubly excited state $|f\rangle$ (see Fig 1B).

Due to the quantum nature of the signal and the idler fields, the interaction of each of these fields with matter

must be at least second order to yield a non vanishing trace in Eq. (5). Therefore, the perturbative expansion of the integral in the exponent of Eq. (5) will contain ten field-matter interactions; six with the sample molecules (two with each of the signal, idler field and pump fields) and the last four are with the detectors. Note that there can be no interactions during the intervals τ_s and τ_i . In that case the field correlation function will vanish since $\hat{a}|0\rangle = 0$. Thus, the leading contribution to Eq. (5) comes from the four diagrams shown in Fig. 2 (for rules see [20]). The coherent part of the signal represented by interaction of two spontaneously generated quantum and one classical modes is proportional to the number of pairs of sites in the sample $\sim N(N-1)$, which dominates the other, incoherent, $\sim N$ response for large N . Details of the calculation of the correlation function (5) are presented in Appendix A. We obtain for the “bare” coincidence rate

$$R_c^{(B)}(\omega_s, \omega'_i, \omega_p, \omega'_p) = N(N-1) \left(\frac{2\pi\hbar}{V} \right)^4 \times \mathcal{E}^{*(p)}(\omega_p) \mathcal{E}^{(p)}(\omega'_p) \mathcal{D}(\omega_s) \mathcal{D}(\omega_p - \omega_s) \mathcal{D}(\omega'_i) \mathcal{D}(\omega'_p - \omega'_i) \times \chi_{LL-}^{(2)}[-(\omega'_p - \omega'_i), -\omega'_i, \omega'_p] \chi_{LL-}^{(2)*}[-\omega_s, -(\omega_p - \omega_s), \omega_p], \quad (7)$$

where $\mathcal{E}^{(p)}(\omega) \equiv E^{(p)}(\omega)\beta^{(p)}$ is a classical field amplitude, $E^{(p)}(\omega)$ is the pump pulse envelope and $\mathcal{D}(\omega) = \omega\tilde{\mathcal{D}}(\omega)$ where $\tilde{\mathcal{D}}(\omega) = V\omega^2/\pi^2c^3$ is the density of radiation modes. For our level scheme (Fig. 1b) the nonlinear susceptibility $\chi_{LL-}^{(2)}$ (see Eq. (3)) is given by

$$2^{-1/2} \chi_{LL-}^{(2)}[-(\omega'_p - \omega'_i), -\omega'_i, \omega'_p] = \frac{1}{\hbar} \frac{\mu_{gf}^* \mu_{fe} \mu_{eg}}{\omega'_p - \omega_{gf} + i\gamma_{gf}} \times \frac{1}{\omega'_p - \omega'_i - \omega_{eg} + i\gamma_{eg}} + (\omega'_i \leftrightarrow \omega'_p - \omega'_i). \quad (8)$$

Eq. (7) represents a 6-mode ($\omega_p, \omega_i, \omega_s, \omega'_p, \omega'_i, \omega'_s$) field-matter correlation function factorized into two generalized susceptibilities each representing the interaction of two quantum and one classical mode with a different molecule. Because of two constraints $\omega_p = \omega_s + \omega_i$, $\omega'_p = \omega'_s + \omega'_i$ that originate from time translation invariance on each of the two molecules that generate the nonlinear response, Eq. (7) only depends on four field modes. Each molecule creates a coherence in the field between states with zero and one photon. By combining the susceptibilities from a pair of molecules we obtain a photon occupation number that can be detected. Thus, the detection process must be described in the joint space of the two molecules and involves the interference of four quantum pathways (two with bra and two with ket) with different time orderings. Note that this pathway information is not explicit in the Langevin approach.

For comparison, if all three fields (signal, idler and pump) are classical, the number of material-field interactions is reduced to three - one for each field. Then

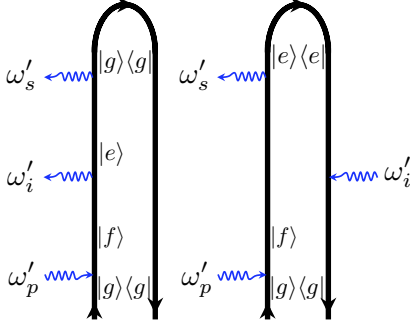


FIG. 4. (Color online) Loop diagrams for the interaction of three classical pump, signal and idler fields. Left and right loop diagrams correspond to the first and second term in Eq. (9), respectively. Each loop has two possible permutations of i/s corresponding to the time ordering between idler and signal photons.

the leading contribution to the field correlation function shown in Fig. 4 yields the semiclassical nonlinear susceptibility $\chi_{+--}^{(2)}$

$$2^{-3/2}\chi_{+--}^{(2)}[-(\omega'_p - \omega'_i), -\omega'_i, \omega'_p] = \frac{1}{\hbar^2}\langle g|\mathcal{T}V_L\mathcal{G}(\omega'_p - \omega'_i)V_L\mathcal{G}(\omega'_p)V_L^\dagger|g\rangle + \frac{1}{\hbar^2}\langle g|\mathcal{T}V_L\mathcal{G}^\dagger(\omega'_i)V_L\mathcal{G}(\omega'_p)V_L^\dagger|g\rangle = \frac{1}{\hbar^2}\frac{\mu_{gf}^*\mu_{fe}\mu_{eg}}{\omega_p - \omega_{gf} + i\gamma_{gf}} \times \left[\frac{1}{\omega_p - \omega'_i - \omega_{eg} + i\gamma_{eg}} + \frac{1}{\omega'_i - \omega_{eg} - i\gamma_{eg}} \right] + (\omega'_i \leftrightarrow \omega_p - \omega'_i), \quad (9)$$

where $\mathcal{G}(\omega) = 1/(\omega - H_{0-}/\hbar + i\gamma)$ is the retarded Liouville Green's function, and γ is lifetime broadening. $\chi_{LL-}^{(2)}$ possesses a permutation symmetry with respect to $s \leftrightarrow i$ (both have L index). In contrast the semiclassical calculation via $\chi_{+++}^{(2)}$ is non symmetric with respect to $s \leftrightarrow i$ (one + and one - indexes), which results in coincidence count rate that depends upon whether the signal or idler detector clicks first [21].

B. Detected coincidence rate

We shall calculate the coincidence rate registered by two detectors - D_s and D_i , whose inputs are located at $r_G^{(s)}$ for a signal and at $r_G^{(i)}$ for an idler. Both detectors consist of a time gate $F_t^{(x)}$ centered at \bar{t}_x followed by a frequency gate $F_f^{(x)}$ centered at $\bar{\omega}_x$ where $x = s, i$ indicates signal or idler. First, the time gate transforms the electric field of the mode x given by $E^{(x)}(r_G^{(x)}, t) = \sum_j E_j^{(x)}(r_G^{(x)}, t)$ with $E_j^{(x)}(r_G^{(x)}, t) = E^{(x)}(r_G^{(x)}, \omega_{xj})e^{-i\omega_{xj}t}$ as follows:

$$E_f^{(x)}(r_G^{(x)}, t) = F_t^{(x)}(t, \bar{t}_x)E^{(x)}(r_G^{(x)}, t). \quad (10)$$

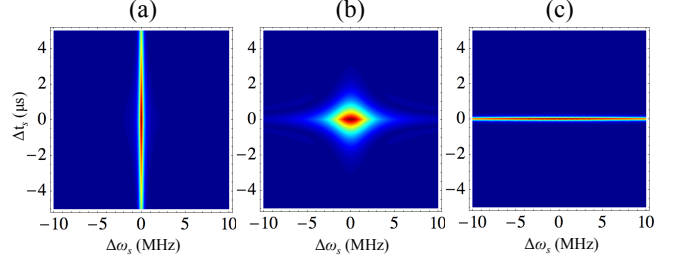


FIG. 5. (Color online) Gating spectrogram (22) for $\gamma_s = \Gamma_s = 0.1\text{MHz}$ - (a), 1MHz - (b), 10MHz - (c).

Then, the frequency gate is applied $E_f^{(x)}(r_G^{(x)}, \omega) = F_f(\omega, \bar{\omega}_x)E_t^{(x)}(r_G^{(x)}, \omega)$ where $E^{(x)}(\omega) = \int_{-\infty}^{\infty} dt e^{i\omega t} E^{(x)}(t)$. We thus obtain the time-and-frequency-gated field $E_{tf}(t)$. We assume that the time gate is applied first. Therefore, the combined detected field at the position r_D can be written as

$$E_{tf}^{(x)}(r_D^{(x)}, t) = \int_{-\infty}^{\infty} dt' F_f^{(x)}(t - t', \bar{\omega}_x) F_t^{(x)}(t', \bar{t}_x) E^{(x)}(r_G^{(x)}, t'), \quad (11)$$

where $E^{(x)}(t) \equiv \sum_j \sqrt{2\pi\hbar\omega_{xj}/V} \hat{a}_{xj} e^{-i\omega_{xj}t}$ (V is a mode quantization volume). For simplicity we omit the position dependence in the fields assuming that propagation between $r_G^{(x)}$ and $r_D^{(x)}$ is included in the spectral gate function.

The measured coincidence rate of photons coming from signal and idler fields is given by Eq. (4). In order to provide a clean bookkeeping for all interactions we describe the bare signal in terms of Liouville space “left” and “right” superoperators [19]

$$\tilde{R}_c^{(B)}(\omega_s, t'_s, \omega'_i, t'_i) = \sum_{s, s'} \sum_{i, i'} \int_0^\infty d\tau_s \int_0^\infty d\tau_i e^{-i\omega_s\tau_s - i\omega'_i\tau_i} \times \langle E_R^{\dagger(i)}(t_i) E_R^{\dagger(s)}(t'_s + \tau_s) E_L^{(s')}(\tau'_s) E_L^{(i)}(t'_i - \tau_i) e^{-\frac{i}{\hbar} \int_{-\infty}^\infty \sqrt{2} H_L(\tau) d\tau} \rangle, \quad (12)$$

where $\sum_s \rightarrow \int d\bar{\omega}_s \tilde{\mathcal{D}}(\bar{\omega}_s)$ with density of radiation modes $\tilde{\mathcal{D}}(\omega) = V\omega^2/\pi^2 c^3$ is understood. We further introduce the Wigner spectrogram for the gate [23]

$$\tilde{W}(\omega'_s, t'_s; \omega'_i, t'_i; \bar{\omega}_s, \bar{t}_s; \bar{\omega}_i, \bar{t}_i) = W^{(s)}(\omega'_s, t'_s; \bar{\omega}_s, \bar{t}_s) W^{(i)}(\omega'_i, t'_i; \bar{\omega}_i, \bar{t}_i), \quad (13)$$

where

$$W^{(s)}(\omega'_s, t'_s; \bar{\omega}_s, \bar{t}_s) = \int_{-\infty}^{\infty} \frac{d\omega_s}{(2\pi)^2} |F_f(\omega_s, \bar{\omega}_s)|^2 W_t^{(s)}(t'_s, \omega_s - \omega'_s, \bar{t}_s), \quad (14)$$

$$W^{(i)}(\omega'_i, t'_i; \bar{\omega}_i, \bar{t}_i) = \int_{-\infty}^{\infty} \frac{d\omega_i}{(2\pi)^2} |F_f(\omega_i, \bar{\omega}_i)|^2 W_t^{(i)}(t'_i, \omega_i - \omega'_i, \bar{t}_i) \quad (15)$$

with

$$W_t^{(s)}(t'_s, \omega_s, \bar{t}_s) = \int_{-\infty}^{\infty} d\tau_s e^{i\omega\tau_s} F_t^{(s)*}(t'_s + \tau_s, \bar{t}_s) F_t^{(s)}(t'_s, \bar{t}_s), \quad (16)$$

$$W_t^{(i)}(t'_i, \omega_i, \bar{t}_i) = \int_{-\infty}^{\infty} d\tau_i e^{i\omega\tau_i} F_t^{(i)*}(t'_i, \bar{t}_i) F_t^{(i)}(t'_i - \tau_i, \bar{t}_i). \quad (17)$$

Taking into account Eq. (A18) we redefine the bare signal according to Eq. (7). We further modify the gating spectrogram that controls the temporal and spectral resolution of the measurement [23]

$$\begin{aligned} W(\omega_s, \omega'_i, \omega_p, \omega'_p; \bar{\omega}_s, \bar{\omega}_i) &= \int_{-\infty}^{\infty} dt_s W^{(s)}(\omega_s, t'_s; \bar{\omega}_s, \bar{t}_s) e^{i(\omega_s + \omega'_i - \omega'_p)t'_s} \\ &\times \int_{-\infty}^{\infty} dt'_i W^{(i)}(\omega'_i, t'_i; \bar{\omega}_i, \bar{t}_i) e^{-i(\omega_s + \omega'_i - \omega_p)t'_i} \end{aligned} \quad (18)$$

Taking Eqs. (4), (7) and (18) into account yields

$$R_c(\bar{\omega}_s, \bar{t}_s; \bar{\omega}_i, \bar{t}_i) = \int_{-\infty}^{\infty} d\omega_s d\omega'_i d\omega_p d\omega'_p R_c^{(B)}(\omega_s, \omega'_i, \omega_p, \omega'_p) \times W(\omega_s, \omega'_i, \omega_p, \omega'_p; \bar{\omega}_s, \bar{t}_s, \bar{\omega}_i, \bar{t}_i). \quad (19)$$

The spectrogram represents the combination of a spectral gate centered at $\bar{\omega}_x$ followed by a time gate centered at \bar{t}_x ($x = s, i$).

In our simulations the spectral gate was taken to be the Fabry-Perot etalon [24], and the time gate is exponential:

$$F_f^{(x)}(\omega_x, \bar{\omega}_x) = \frac{\gamma_x}{\gamma_x - i(\omega_x - \bar{\omega}_x)}, \quad (20)$$

$$F_t^{(x)}(t_x, \bar{t}_x) = e^{-\Gamma_x(t_x - \bar{t}_x)}. \quad (21)$$

The Wigner spectrogram for this gate is then given by

$$\begin{aligned} W^{(s)}(\Delta\omega_s; \Delta t_s) &= \frac{1}{2\pi} \frac{e^{-\Gamma_s \Delta t_s}}{\frac{\Delta\omega_s}{\gamma_s} + i \left(1 - \frac{\Gamma_s}{\gamma_s}\right)} \times \\ &\left[\frac{e^{-\Gamma_s \Delta t_s}}{\frac{\Delta\omega_s}{\gamma_s} - i \left(1 + \frac{\Gamma_s}{\gamma_s}\right)} + \frac{e^{(i\Delta\omega_s - \gamma_s)\Delta t_s}}{\frac{\Delta\omega_s}{\Gamma_s} + i \left(1 + \frac{\Gamma_s}{\gamma_s}\right)} \right], \end{aligned} \quad (22)$$

where $\Delta\omega_s = \omega'_s - \bar{\omega}_s$ and $\Delta t_s = t'_s - \bar{t}_s$. Clearly, the Wigner spectrogram (22) couples the time and frequency resolution which are now correlated via the Fourier uncertainty. Thus, increasing (decreasing) γ_s and Γ_s enhance (suppress) the frequency uncertainty and suppress (enhance) the time uncertainty (see Fig. 5).

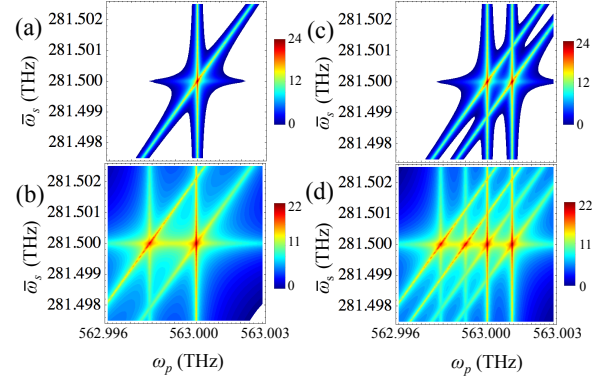


FIG. 6. (Color online) Left column: two dimensional coincidence counting rate (log scale in arb. units) calculated using quantum theory Eq. (19) assuming a single monochromatic pump with frequency ω_p . Idler detector resonant with intermediate level $\bar{\omega}_i = \omega_{eg} = 282\text{THz}$ - panel (a), while $\omega_{eg} - \bar{\omega}_i = 2\text{GHz}$ for (b). Right column: same as left but for a pump made out of two monochromatic beams with frequencies $\omega_p - \omega'_p = 2 \cdot 10^{-6}\omega_p$.

III. EXPERIMENTAL SIMULATIONS

Fig. 3 compares both susceptibilities calculated for a typical KTP crystal (PPKTP) represented by a degenerate three-level system with $\lambda_{eg} = 2\lambda_{gf} = 1064\text{nm}$ [22]. The experimental lifetime broadening of the single and two-photon resonances is 16MHz and 40 MHz, respectively [22]. Fig. 3c,e,g show that far from resonances ($\omega_i \neq \omega_{eg}$, $\omega_p \neq \omega_{gf}$) the semiclassical and quantum susceptibilities coincide and depend weakly on the frequencies ω_p and ω_i . This is the regime covered by the semiclassical theory, where the susceptibility is assumed to be a constant. Similar agreement between classical and quantum susceptibilities can be observed if the pump is resonant with two-photon transition $\omega_p \simeq \omega_{gf}$ but the idler is off resonance $\omega_i \neq \omega_{eg}$ - Fig. 3d,f,h. However, close to resonance - Fig. 3a,b the two susceptibilities are very different. The semiclassical susceptibility $\chi_{+--}^{(2)}$ vanishes at resonance, where the quantum susceptibility $\chi_{LLL-}^{(2)}$ reaches its maximum.

To put the present ideas into more practical perspective we show in Fig. 6 the coincidence count rate for a monochromatic pump ω_p and mean signal detector frequency $\bar{\omega}_s$. The quantum theory yields one strong resonant peak at $\bar{\omega}_s = \omega_p - \omega_{eg}$ and two weak peaks at $\omega_p = \omega_{gf}$ and $\bar{\omega}_s = \omega_{eg}$ if the idler detector is resonant with the intermediate state $|e\rangle$: $\bar{\omega}_i = \omega_{eg}$ - Fig. 6a. However, if we tune the idler detector to a different frequency, for instance $\omega_{eg} - \bar{\omega}_i = 2\text{GHz}$ there is an additional peak at $\bar{\omega}_s = \omega_p - \bar{\omega}_i$ - Fig. 6b. Similarly, when the pump consists of two monochromatic beams $\omega_p \neq \omega'_p$ (panels C,D) the number of peaks are doubled compare to single monochromatic pump. Clearly, one can reproduce the exact same peaks for ω'_p as for ω_p .

Shwartz et al. recently reported PDC in diamond,

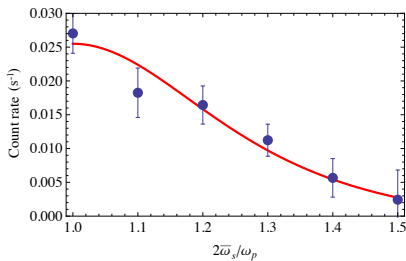


FIG. 7. (Color online) Simulated coincidence count rate in Eq. (19) vs $2\bar{\omega}_s/\omega_p$. $\bar{\omega}_s$ and $\omega_p/2$ is the mean frequency of the signal detector and the degenerate photon frequency, respectively. Dots represent the experimental results of Shwartz et al. [21].

where 18keV pump field generates two X-ray photons [21]. They have shown that the semiclassical calculation without Langevin noise agrees with experiment only far from degeneracy $\bar{\omega}_s \gg \omega_p/2$ but yields a factor of two smaller count rate close to degenerate frequency $\bar{\omega}_s = \omega_p/2$ and strongly depends on which detectors register the photon first. To overcome this problem they added a Langevin noise to take into account other vacuum modes. Our calculation (solid line in Fig. 7) reproduces experiment (dots) in the entire frequency range without adding noise. The noise comes from the summation over ω_s , ω'_s , ω_i and ω'_i . In simulations we assumed $\omega_{eg} = 280\text{eV}$, $\omega_p = \omega'_p = 18\text{keV}$, and fixed the idler detector position at $\bar{\omega}_i = 9\text{keV}$, which corresponds to off resonant parameter regime. Therefore, the result is independent of the frequency variations of the susceptibility. Fig. 7 rather illustrates the photon detection treated in the joined space of two sites.

IV. CONCLUSIONS

In summary, a microscopic theory of the photon counting in PDC that applied to resonant as well as off resonant frequencies reveals that it is given by a sum over

$$\langle \mathbf{E}(t_{10}, \dots, t_1) \rangle = \langle \mathcal{T} E_R^{\dagger(s_{10})}(t_{10}) E_L^{(s_9)}(t_9) E_R^{\dagger(i_8)}(t_8) E_L^{(i_7)}(t_7) E_L^{\dagger(s_6)}(t_6) E_R^{(s_5)}(t_5) E_L^{\dagger(i_4)}(t_4) E_R^{(i_3)}(t_3) E_R^{\dagger(p_2)}(t_2) E_L^{(p_1)}(t_1) \rangle, \quad (\text{A1})$$

where $t_{10} = t'_s + \tau_s$, $t_9 = t'_s$, $t_8 = t'_i$, $t_7 = t'_i - \tau_i$ are the interaction times with the detection. We can factorize Eq. (A1) into the product of signal, idler and pump correlation functions, which yields

$$\langle \mathbf{E}(t_{10}, \dots, t_1) \rangle = \langle \mathbf{E}^{(s)}(t_{10}, t_9, t_6, t_5) \rangle \langle \mathbf{E}^{(i)}(t_8, t_7, t_4, t_3) \rangle \times \langle \mathbf{E}^{(p)}(t_2, t_1) \rangle, \quad (\text{A2})$$

6-mode paths that involves a pair of molecules in the sample. Two constraints $\omega_p = \omega_s + \omega_i$, $\omega'_p = \omega'_s + \omega'_i$ reduce the number of independent frequency modes to four. The correct photon statistics due to the presence of multiple signal and idler vacuum modes is reproduced. The time and frequency resolution of the measurement is controlled by the gate parameters.

ACKNOWLEDGMENTS

We would like to thank Prof. S.E. Harris and Dr. S. Shwartz for sharing their experimental results and useful discussions. We gratefully acknowledge the support of the National Science Foundation through Grant No. CHE-1058791 and computations are supported by CHE-0840513, the Chemical Sciences, Geosciences and Biosciences Division, Office of Basic Energy Sciences, Office of Science, US Department of Energy.

Appendix A: Calculation of the bare coincidence rate

Since initially both signal and idler modes are in the vacuum state $|0\rangle\langle 0|$ and the final state is $|1\rangle\langle 1|$, the interaction of each of these fields with matter that yields a non vanishing trace must be at least second order. Therefore, the perturbative expansion of the integral in the exponent of Eq. (5) will contain ten field-matter interactions (six with the sample and four with the detectors). The number of diagrams is reduced by noting that two interactions occur with each of the pump, signal, and idler fields. Another simplification arises since there can be no interactions during the interval τ_s and τ_i , since in that case the field correlation function will vanish since $\hat{a}|0\rangle = 0$. Finally, since the signal and idler fields are initially in the vacuum state the correct combination of the fields must be $E_R^{(x)}(t)E_L^{\dagger(x)}(t')$.

The leading contribution to the field correlation function shown in Fig. 2 is thus given by the time ordered superoperator correlation function

where

$$\begin{aligned} & \langle \mathbf{E}^{(s)}(t_{10}, t_9, t_6, t_5) \rangle \\ &= f^{(s)*}(\omega_{10}^{(s)}) f^{(s)}(\omega_9^{(s)}) f^{(s)*}(\omega_6^{(s)}) f^{(s)}(\omega_5^{(s)}) \\ & \times e^{i\omega_{10}^{(s)} t_{10} - i\omega_9^{(s)} t_9 + i\omega_6^{(s)} t_6 - i\omega_5^{(s)} t_5} \langle 0 | \hat{a}_R^{\dagger s_{10}} \hat{a}_L^{s_9} \hat{a}_L^{\dagger s_6} \hat{a}_R^{s_5} | 0 \rangle, \end{aligned} \quad (\text{A3})$$

$f(\omega) = \sqrt{2\pi\hbar\omega/V}$. Note, that the matrix element in Eq. (A3) is

$$\langle 0|\hat{a}_R^{\dagger s_{10}}\hat{a}_L^s\hat{a}_L^{\dagger s_6}\hat{a}_R^{s_5}|0\rangle = \langle 0|\hat{a}_L^{s_5}\hat{a}_L^{\dagger s_{10}}\hat{a}_L^{s_9}\hat{a}_L^{\dagger s_6}|0\rangle = \delta_{s_5,s_{10}}\delta_{s_9,s_6}, \quad (\text{A4})$$

this implies that only certain pairs of modes yield nonzero correlation functions. Taking into account that the mode frequencies are given by $\omega_{10}^{(s)} = \omega_s$, $\omega_9^{(s)} = \omega_s - \Omega_s$, $\omega_8^{(s)} = \omega'_i + \Omega_i$, $\omega_7^{(i)} = \omega'_i$ Eq. (A3) yields

$$\langle \mathbf{E}^{(s)}(t_{10}, t_9, t_6, t_5) \rangle = |f(\omega_s)|^2 |f(\omega_s - \Omega_s)|^2 e^{i\omega_s(t_{10}-t_5)+i(\omega_s-\Omega_s)(t_6-t_9)}. \quad (\text{A5})$$

For the idler we similarly get

$$\langle \mathbf{E}^{(i)}(t_8, t_7, t_4, t_3) \rangle = |f(\omega'_i + \Omega_i)|^2 |f(\omega'_i)|^2 e^{-i(\omega'_i+\Omega_i)(t_3-t_8)-i\omega'_i(t_7-t_4)}. \quad (\text{A6})$$

The two-point pump correlation function is given by

$$\langle \mathbf{E}^{(p)}(t_2, t_1) \rangle = \frac{1}{(2\pi)^2} \int_{-\infty}^{\infty} d\omega_p d\omega'_p \mathcal{E}^{(p)*}(\omega_p) \mathcal{E}^{(p)}(\omega'_p) e^{i\omega_p t_2 - i\omega'_p t_1}, \quad (\text{A7})$$

where the classical field amplitude $\mathcal{E}^{(p)}(\omega) \equiv E^{(p)}(\omega)\beta^{(p)}$ with pump pulse represented by the envelope $E^{(p)}(\omega)$. Combining Eqs. (A5), (A6) and (A7), yields the total field correlation function

$$\langle \mathbf{E}(t_{10}, \dots, t_1) \rangle = \frac{1}{(2\pi)^2} \int_{-\infty}^{\infty} d\omega_p d\omega'_p |f(\omega_s)|^2 |f(\omega_s - \Omega_s)|^2 |f(\omega'_i + \Omega_i)|^2 |f(\omega'_i)|^2 \times \mathcal{E}^{(p)*}(\omega_p) \mathcal{E}^{(p)}(\omega'_p) e^{i\omega_s(t_{10}-t_5)+i(\omega_s-\Omega_s)(t_6-t_9)} e^{-i(\omega'_i+\Omega_i)(t_3-t_8)-i\omega'_i(t_7-t_4)} e^{i\omega_p t_2 - i\omega'_p t_1}. \quad (\text{A8})$$

We neglect all propagation effects and assume that the detectors are located in close proximity to the sample. The corresponding 6-point correlation function of the sample molecules is given by

$$\langle \mathbf{V}(t_6, \dots, t_1) \rangle = \langle \mathcal{T} V_L^{(s)}(t_6) V_L^{(i)}(t_4) V_L^{\dagger(p)}(t_1) \rangle_1 \times \langle \mathcal{T} V_R^{\dagger(s)}(t_5) V_R^{\dagger(i)}(t_3) V_R^{(p)}(t_2) \rangle_2. \quad (\text{A9})$$

The coherent part of the signal represented by interaction of two spontaneously generated quantum and one classical modes results in the emission of signal and idler modes into a cone of solid angle $\Delta\mathbf{k}$. Here the phase mismatch $\Delta\mathbf{k} = \mathbf{k}_p - \mathbf{k}_s - \mathbf{k}_i$ represent the uncertainty of the phase which is reciprocal of the characteristic sample size. This implies that the phase matched two molecule

contribution

$$\sum_{m=1}^N \sum_{n=1}^{N-1} e^{i\Delta\mathbf{k}(\mathbf{r}-\mathbf{r}_m)} e^{i\Delta\mathbf{k}(\mathbf{r}-\mathbf{r}_n)} \simeq N(N-1) \quad (\text{A10})$$

dominates the other, incoherent, single molecule $\sim N$ response for large N . For comparison, the incoherent response given by $\chi^{(5)}$ has $\sim N$ - scaling. Here

$$\Delta\mathbf{k} = -\mathbf{k}_{10}^{(s)} + \mathbf{k}_9^{(s)} - \mathbf{k}_8^{(i)} + \mathbf{k}_7^{(i)} - \mathbf{k}_6^{(s)} + \mathbf{k}_5^{(s)} + \mathbf{k}_4^{(i)} - \mathbf{k}_3^{(i)} - \mathbf{k}_2^{(p)} + \mathbf{k}_1^{(p)}. \quad (\text{A11})$$

We can now calculate the entire correlation function

$$\langle \mathcal{T} E_R^{\dagger(i)}(t_i) E_R^{\dagger(s)}(t_s + \tau_s) E_L^{(s')}(t_s) E_L^{(i')}(t_i - \tau_i) e^{-\frac{i}{\hbar} \int_{-\infty}^{\infty} \sqrt{2} H_{\text{int}}(\tau) d\tau} \rho(-\infty) \rangle = \frac{N(N-1)}{(2\pi)^2} \left(-\frac{i\sqrt{2}}{\hbar} \right)^6 \int_{-\infty}^{\infty} d\omega_p d\omega'_p |f(\omega_s)|^2 |f(\omega_s - \Omega_s)|^2 |f(\omega'_i + \Omega_i)|^2 |f(\omega'_i)|^2 \mathcal{E}^{(p)*}(\omega_p) \mathcal{E}^{(p)}(\omega'_p) \Xi, \quad (\text{A12})$$

where

$$\Xi = \int_{-\infty}^{\infty} dt_6 dt_5 dt_4 dt_3 dt_2 dt_1 e^{i\omega_s(t_s+\tau_s-t_5)+i(\omega_s-\Omega_s)(t_6-t_5)} e^{-i(\omega'_i+\Omega_i)(t_3-t_i)-i\omega'_i(t_i-\tau_i-t_4)} e^{i\omega_p t_2 - i\omega'_p t_1} \times \langle g | \mathcal{T} V_L^{(s)} \mathcal{G}(t_6 - t_4) V_L^{(i)} \mathcal{G}(t_4 - t_1) V_L^{\dagger(p)} | g \rangle \cdot \langle g | \mathcal{T} V_R^{\dagger(s)} \mathcal{G}^\dagger(t_5 - t_3) V_R^{\dagger(i)} \mathcal{G}^\dagger(t_3 - t_2) V_R^{(p)} | g \rangle. \quad (\text{A13})$$

To evaluate Ξ we must take into account all possible time orderings of t_1, \dots, t_6 . This gives four terms $\Xi = \Xi_a + \Xi_b +$

$\Xi_c + \Xi_d$ represented by the loop diagrams as marked in Fig. 2

$$\begin{aligned} \Xi_a = & e^{i\omega_s\tau_s + i\Omega_s t_s + i\omega'_i\tau_i + i\Omega_i t_i} \delta(\omega'_p - \omega'_i - \omega_s + \Omega_s) \delta(\omega_p - \omega'_i - \omega_s - \Omega_i) \\ & \times \langle g | V_L \mathcal{G}(\omega'_p - \omega'_i) V_L \mathcal{G}(\omega'_p) V_L^\dagger | g \rangle \cdot \langle g | V_L \mathcal{G}^\dagger(\omega_p) V_L^\dagger \mathcal{G}^\dagger(\omega_p - \omega_s) V_L^\dagger | g \rangle, \end{aligned} \quad (\text{A14})$$

$$\begin{aligned} \Xi_b = & e^{i\omega_s\tau_s + i\Omega_s t_s + i\omega'_i\tau_i + i\Omega_i t_i} \delta(\omega'_p - \omega'_i - \omega_s + \Omega_s) \delta(\omega_p - \omega'_i - \omega_s - \Omega_i) \\ & \times \langle g | V_L \mathcal{G}(\omega'_i) V_L \mathcal{G}(\omega'_p) V_L^\dagger | g \rangle \cdot \langle g | V_L \mathcal{G}^\dagger(\omega_p) V_L^\dagger \mathcal{G}^\dagger(\omega_p - \omega_s) V_L^\dagger | g \rangle, \end{aligned} \quad (\text{A15})$$

$$\begin{aligned} \Xi_c = & e^{i\omega_s\tau_s + i\Omega_s t_s + i\omega'_i\tau_i + i\Omega_i t_i} \delta(\omega'_p - \omega'_i - \omega_s + \Omega_s) \delta(\omega_p - \omega'_i - \omega_s - \Omega_i) \\ & \times \langle g | V_L \mathcal{G}(\omega'_p - \omega'_i) V_L \mathcal{G}(\omega'_p) V_L^\dagger | g \rangle \cdot \langle g | V_L \mathcal{G}^\dagger(\omega_p) V_L^\dagger \mathcal{G}^\dagger(\omega_s) V_L^\dagger | g \rangle, \end{aligned} \quad (\text{A16})$$

$$\begin{aligned} \Xi_d = & e^{i\omega_s\tau_s + i\Omega_s t_s + i\omega'_i\tau_i + i\Omega_i t_i} \delta(\omega'_p - \omega'_i - \omega_s + \Omega_s) \delta(\omega_p - \omega'_i - \omega_s - \Omega_i) \\ & \times \langle g | V_L \mathcal{G}(\omega'_i) V_L \mathcal{G}(\omega'_p) V_L^\dagger | g \rangle \cdot \langle g | V_L \mathcal{G}^\dagger(\omega_p) V_L^\dagger \mathcal{G}^\dagger(\omega_s) V_L^\dagger | g \rangle. \end{aligned} \quad (\text{A17})$$

Combining Eqs. (A14) - (A17) we can connect the signal to the nonlinear susceptibility $\chi_{LL-}^{(2)}$,

$$\begin{aligned} & \langle \mathcal{T} E_R^\dagger(i)(t_i) E_R^\dagger(s)(t_s + \tau_s) E_L^{(s')}(t_s) E_L^{(i')}(t_i - \tau_i) e^{-\frac{i}{\hbar} \int_{-\infty}^{\infty} \sqrt{2} H_{\text{int}}(\tau) d\tau} \rho(-\infty) \rangle \\ & = N(N-1) \left(\frac{2\pi\hbar}{V} \right)^4 \int_{-\infty}^{\infty} \frac{d\omega_p}{2\pi} \frac{d\omega'_p}{2\pi} \mathcal{E}^{(p)*}(\omega_p) \mathcal{E}^{(p)}(\omega'_p) \\ & \times \omega_s \omega'_i (\omega_s - \Omega_s) (\omega'_i + \Omega_i) \delta(\omega_s + \omega'_i + \Omega_i - \omega_p) \delta(\omega_s - \Omega_s + \omega'_i - \omega_p) e^{i\omega_s\tau_s + i\Omega_s t_s + i\omega'_i\tau_i + i\Omega_i t_i} \\ & \times \chi_{LL-}^{(2)}[-(\omega'_p - \omega'_i), -\omega'_i, \omega'_p] \cdot \chi_{LL-}^{(2)*}[-(\omega_p - \omega_s), -\omega_s, \omega_p], \end{aligned} \quad (\text{A18})$$

where

$$\begin{aligned} & 2^{-1/2} \chi_{LL-}^{(2)}[-(\omega'_p - \omega'_i), -\omega'_i, \omega'_p] \\ & = \frac{1}{\hbar} \langle g | \mathcal{T} V_L \mathcal{G}(\omega'_p - \omega'_i) V_L \mathcal{G}(\omega'_p) V_L^\dagger | g \rangle + \frac{1}{\hbar^2} \langle g | \mathcal{T} V_L \mathcal{G}(\omega'_i) V_L \mathcal{G}(\omega'_p) V_L^\dagger | g \rangle \\ & = \frac{1}{\hbar} \frac{\mu_{gf}^* \mu_{fe} \mu_{eg}}{\omega'_p - \omega_{gf} + i\gamma_{gf}} \left[\frac{1}{\omega'_i - \omega_{eg} + i\gamma_{eg}} + \frac{1}{\omega'_p - \omega'_i - \omega_{eg} + i\gamma_{eg}} \right], \end{aligned} \quad (\text{A19})$$

where μ_{ij} , γ_{ij} , and ω_{ij} are dipole moment, line width and transition frequency corresponding to a given transition $i \leftrightarrow j$. Note, that $\chi_{LL-}^{(2)}$ is different from the semiclassical $\chi_{+--}^{(2)}$. Physically, this is clear, since $\chi_{LL-}^{(2)} = \frac{1}{2}(\chi_{+--}^{(2)} + \chi_{+-+}^{(2)})$ is symmetric with respect to permutation of $s \leftrightarrow i$, while the classical result of $\chi_{+--}^{(2)}$ is not (ω_s is “+” and ω_i is “-”). This can be seen by comparing (A19) and (9).

If the energies of the signal ω_s and idler ω'_i are far from the degenerate values $\omega_p/2$ and $\omega'_p/2$, respectively, then for $\omega_s \gg \omega_p - \omega_s$ and $\omega'_i \gg \omega'_p - \omega'_i$, then the $\chi_{+--}^{(2)}$ coincides with $\chi_{LL-}^{(2)}$ (see Ref. [20]). Furthermore, if signal and idler have only single mode components, then phase matching yields $\delta(\omega_s + \omega'_i - \omega_p)$ with $\omega_p = \omega'_p$ so that the result is governed by $|\chi_{LL-}^{(2)}[-(\omega_p - \omega'_i), -\omega'_i, \omega_p]|^2$ (Ref. [20]).

To gain deeper physical insight we note, that Eq. (A18) is expressed as a convolution of two generalized nonlinear susceptibilities $\chi_{LL-}^{(2)}$ calculated in the joined field-matter space of two molecules. This description is similar to a transition amplitude approach that is often used in homodyne detection. The field wave function

$$|\psi\rangle = |0\rangle + \sum_{i,s} T(i,s) \hat{a}_i^\dagger \hat{a}_s^\dagger |0\rangle, \quad (\text{A20})$$

where the transition amplitude $T(s,i)$ is given by

$$\begin{aligned} T(i,s) = & \sqrt{\frac{2\pi\hbar\omega_s}{V}} \sqrt{\frac{2\pi\hbar\omega_i}{V}} \int_{-\infty}^{\infty} \frac{d\omega_p}{2\pi} \mathcal{E}^{(p)}(\omega_p) \\ & \times \delta(\omega_s + \omega_i - \omega_p) \chi_{LL-}^{(2)}[-\omega_s, -\omega_i, \omega_p] \end{aligned} \quad (\text{A21})$$

can be rewritten as a sum of two terms that represent two pathways (i arrives first or s arrives first). The field density matrix $|\psi\rangle\langle\psi|$ has 4 pathways - two for the bra and

two for the ket (see Fig. 2). The gating must be described by the density matrix in the joint space of two molecules and it involves the interference of all 4 pathways. In other words since each $\chi_{LL-}^{(2)}$ depends on the signal, idler and pump, one cannot say that the signal and idler are generated at different molecules. Rather, each molecule creates a coherence in the field between states with zero and one photon, and by combining the amplitudes from a pair of molecules we get a photon occupation number that can subsequently be further detected.

-
- [1] A. Einstein, B. Podolsky, and N. Rosen, *Phys. Rev.* **47**, 777 (1935).
- [2] For review on PDC theory see: W.H. Louisell, A. Yariv, and A.E. Siegman, *Phys. Rev.* **124**, 1646 (1961); L. Mandel and E. Wolf, *Optical Coherence and Quantum Optics* (Cambridge University Press, Cambridge, 1995); D. Klyshko, *Photons and Nonlinear Optics* (Gordon and Breach, New York, 1988)
- [3] For experimental PDC demonstration see S.E. Harris, M.K. Oshman, and R.L. Byer, *Phys. Rev. Lett.* **18**, 732 (1967); R.L. Byer and S.E. Harris, *Phys. Rev.* **168**, 1064 (1968).
- [4] S.L. Braunstein, H.J. Kimble, *Phys. Rev. A* **61**, 042302(2000); S. Lloyd, S.L. Braunstein, *Phys. Rev. Lett.* **82**, 1784 (1999); S.L. Braunstein, *Nature* **394**, 47 (1998).
- [5] A.I. Lvovsky and M.G. Raymer, *Rev. Mod. Phys.* **81**, 299 (2009).
- [6] V. Giovannetti, S. Lloyd, and L. Maccone, *Phys. Rev. Lett.* **96**, 010401 (2006).
- [7] A.F. Abouraddy, B.E.A. Saleh, A.V. Sergienko, and M.C. Teich, *Opt. Exp.* **9**, 498 (2001).
- [8] T. Jennewein, C. Simon, G. Weihs, H. Weinfurter, and A. Zeilinger, *Phys. Rev. Lett.* **84**, 4729 (2000).
- [9] A.N. Boto, P. Kok, D.S. Abrams, S.L. Braunstein, C.P. Williams, J.P. Dowling, *Phys. Rev. Lett.* **85**, 2733 (2000).
- [10] G.S. Agarwal, R.W. Boyd, E. M. Nagasako, and S. J. Bentley, *Phys. Rev. Lett.* **86**, 1389 (2001).
- [11] E. A. Sete, K. E. Dorfman, and J. P. Dowling, *J. Phys. B* **44**, 225504 (2011).
- [12] C. Gerry and P. Knight, *Introductory Quantum Optics* (Cambridge University Press, Cambridge, 2005).
- [13] M.O. Scully and M.S. Zubairy, *Quantum Optics* (Cambridge University Press, Cambridge, UK, 1997).
- [14] R. Glauber *Quantum Theory of Optical Coherence: Selected Papers and Lectures*(Wiley-VCH, Weinheim, 2007).
- [15] M. Avenhaus, H.B. Coldenstrodt-Ronge, K. Laiho, W. Mauerner, I.A. Walmsley, and C. Silberhorn, *Phys. Rev. Lett.* **101**, 053601 (2008).
- [16] S. Mukamel *Principles of Nonlinear Optical Spectroscopy* (Oxford University Press, New York, 1995).
- [17] R. Lettow, Y.L.A. Rezus, A. Renn, G. Zumofen, E. Ikkonen, S. Götzinger, and V. Sandoghdar, *Phys. Rev. Lett.* **104** 123605 (2010); K. Lee, M. R. Sprague, B.J. Sussman, J. Nunn, N.K. Langford, X.-M. Jim, T. Champion, P. Michelberger, K.F. Reim, D. England, D. Jaksch, and I.A. Walmsley, *Science* **334** 1253 (2011).
- [18] B.E.A. Saleh, B.M. Jost, H.-B. Fei and M.C. Teich, *PRL* **80**, 3483 (1998); *Procedia Chemistry: 22nd Solvay Conference on Chemistry* ed. By G.R. Fleming, G.D. Scholes and A.De Wit, vol. **3** Issue 1 pp. 1-366 (Elsivier 2011).
- [19] K.E. Dorfman and S. Mukamel, *Phys. Rev. A* **86**, 013810 (2012).
- [20] O. Roslyak and S. Mukamel, *Molecular Physics* **107**, 265 (2009).
- [21] S. Shwartz, R.N. Coffee, J.M. Feldkamp, Y. Feng, J.B. Hastings, G.Y. Yin, and S.E. Harris, *Phys. Rev. Lett.* (in press).
- [22] L.-A. Wu, H.J. Kimble, J.L. Hall, and H. Wu, *Phys. Rev. Lett.* **57**, 2520 (1986); V.D. Auria, S. Fornaro, A. Porzio, E.A. Sete, S. Solimeno, *Appl. Phys. B* **91**, 309 (2008).
- [23] A.M. Weiner, *Ultrafast Optics* (Wiley, New York, 2009).
- [24] H. Stolz, *Time-Resolved Light Scattering from Excitons*, *Springer Tracts in Modern Physics*, **130** (Springer-Verlag, Berlin 1994)